Ocean Response and Feedback to the SST Dipole in the Tropical Atlantic[*]

Terrence M. Joyce

Woods Hole Oceanographic Institution, Woods Hole, Massachusetts

Claude Frankignoul

Pierre et Marie Curie University, Paris, France

Jiayan Yang

Woods Hole Oceanographic Institution, Woods Hole, Massachusetts

Helen E. Phillips

Commonwealth Scientific and Industrial Research Organisation, Hobart, Tasmania, Australia

ABSTRACT

The equatorial SST dipole represents a mode of climate variability in the tropical Atlantic Ocean that is closely tied to cross-equatorial flow in the atmosphere, from the cold to the warm hemisphere. It has been suggested that this mode is sustained by a positive feedback of the tropical winds on the cross-equatorial SST gradient. The role, if any, of the tropical ocean is the focus of this investigation, which shows that at the latitudes of the SST signal (centered on 10°N/S) there is a weak positive feedback suggested in data from the last half century, that the cross-equatorial wind stress is closely coupled to this SST gradient on monthly time scales with no discernable lag, and that the period from January to June is the most active period for coupling. Northward (southward) anomalies of cross-equatorial wind stress are associated with a substantial negative (positive) wind stress curl. This wind system can thus drive a cross-equatorial Sverdrup transport in the ocean from the warm to the cold side of the equator (opposite the winds) with a temporal lag of only a few months. The oceanic observations of subsurface temperature and a numerical model hindcast also indicate a clear relationship between this mode of wind-driven variability and changes in the zonal transport of the North Equatorial Countercurrent. It is estimated that the time-dependent oceanic flow is capable of providing a significant contribution to the damping of the SST dipole but that external forcing is essential to sustaining the coupled variability.

1. Introduction

The SST dipole is a ubiquitous feature in tropical Atlantic Ocean variability. It is a statistical mode that captures a significant amount of tropical SST variability to the north and south of the equator and is characterized by amplitudes of opposite sign on either side of the equator extending to latitudes of ±25°. However, its relevance as a "dynamical" mode of variability is in question. It is viewed by some as an important dynamical driver of the tropical atmospheric circulation: shift-ing the position of the ITCZ and causing changes in rainfall in the Nordeste (Moura and Shukla 1981; Nobre and Shukla 1996) and the Sahel (Hastenrath 1990), altering the oceanic heating through adjustments in the trades (Chang et al. 1997, 2000, 2001; Carton et al. 1996; Xie 1999) so as to positively feed back on the SST signal: this is the so-called wind evaporation SST (WES) feedback. Others (Sutton et al. 2000; Czaja et al. 2002; Frankignoul and Kestenare 2002) have not seen any evidence for positive feedback of SST on the overlying atmosphere, and there is a third group who question the dipole (or hemispheric SST gradient) as a dynamic or even statistical mode at all (Houghton and Tourre 1992; Enfield and Mayer 1997; Mehta 1998; Dommenget and Latif 2000). Sources of external influence on the SST in the tropical Atlantic have extended from the North Atlantic Oscillation (NAO) in the North Atlantic to ENSO in the tropical Pacific Ocean to ice cover in the Ross Sea (Mélice and Servain 2003). It can

Corresponding author address: Terrence M. Joyce, Woods Hole Oceanographic Institution, 360 Woods Hole Rd., MS 21, Woods Hole, MA 02543.
E-mail: tjoyce@whoi.edu

be demonstrated from the SST data themselves that there is little correlation between the SST centers to the north and south of the equator. The dynamics we discuss below does not depend on this; it merely relies on there being a SST *difference* between the two regions. While much attention has been given to the SST, the tropical Atlantic Ocean circulation has received little notice in the literature by comparison. Indeed, Czaja et al. (2002) and Seager et al. (2001) found little if any role of ocean circulation in their diagnostic studies of tropical SST variability.

Chang et al. (1997) considered that the mean interhemispheric ocean circulation would provide the negative feedback to balance the positive WES feedback and give rise to oscillations, although subsequent studies have shown that the WES feedback is probably not strong enough to produce self-sustained oscillations. Yang (1999) considered extratropical influences due to high-latitude watermass formation as giving rise to cross-equatorial flow variability and the creation of an SST gradient by advection, not air–sea exchange at all. What makes the study of ocean circulation an important issue is that the interannual SST signal, when compared with the interannual heat flux forcing, shows little correlation in the deep Tropics, even a negative correlation near the African coast, suggesting that in some regions ocean advection is important in creating SST signals that are then damped by the atmosphere. In this effort, we seek to examine annual and interannual variability in the Tropics with an oceanic bias, using the subsurface thermal data together with SST and surface meteorology from the National Centers for Environmental Prediction (NCEP) reanalysis, and the interannual variability in a 40-yr simulation using the ocean component of the global National Center for Atmospheric Research (NCAR) Community Climate System Model (CCSM), hereinafter referred to as NCOM (NCAR CCSM Ocean Model). Our interest is to focus on cross-equatorial flows in the atmosphere and ocean and their effects on SST, upper-ocean heat content, and zonal ocean circulation in the deep Tropics.

We organize this study as follows: a brief description of datasets and model output is followed by an analysis of meridional, cross-equatorial winds and various quantities whose variability is closely correlated with these winds. This is then followed by a discussion of important leads/lags using a dipole index with monthly resolution. The cross-equatorial wind-driven transport is then estimated and discussed as a forced response due to the SST dipole. A 1.5-layer numerical model is presented to illustrate the ocean response to cross-equatorial winds. The cross-equatorial *meridional* ocean flow is shown to be dominant in the interannual variability of the eastward *zonal* flow of the North Equatorial Countercurrent (NECC) as evident in Sverdrup dynamics, the heat content variability of the upper ocean in observations, and NCOM. Last, the overall affect of the time dependent ocean advection on the SST field is consid-ered; the response is one of a negative oceanic feedback on the cross-equatorial SST index, and the strength of this feedback is then estimated using two different models for the advection.

2. Sources of data and model output

Our observations make use of the MBT and XBT files collected and made available in WOD98-05 (Conkright et al. 1998) and online data available through the Global Temperature and Salinity Pilot Project (GTSPP at http://www.nodc.noaa.gov/GTSPP/). While there is rough seasonal XBT sampling presently in the Tropics, we have chosen to examine only annual means and their interannual variability for the subsurface ocean variables in this work. However, we have had to remove seasonal sampling biases before estimating annual averages of temperature at specified depths (see the appendix for further discussion). While this procedure follows a similar one reported by White (1995), we seek only to remove an annual signal and make no attempt for anything other than annual resolution. Because of lack of sufficient data in some regions, this was not uniformly possible everywhere.

In order to achieve the longest possible time series of subsurface temperature data, consistent with the other fields used, we limited our analyses to the upper 150 m, encompassing the MBT data, which are depth limited yet remain the primary measurements prior to the 1970s. In Fig. 1 we show the mean temperature over a 49-yr period as seen in the SST, and selected subsurface (50, 100, 150 m) levels. We also use these four levels to define the heat content (or vertically averaged temperature) for the upper 150 m (see Fig. 1, lower panel) of the ocean using a simple trapezoidal integration scheme from the surface downward. The mean temperature structure bears a remarkable resemblance to the mean surface dynamic height (relative to 500 dbar) from the Merle and Arnault (1985, their Fig. 6) climatology up through 1978. In some parts of the domain, the 150-m level is not below the thermocline and estimated heat content changes will not capture the full effect of thermocline depth variability. However, the paucity of deeper data in the early part of the record gave us a choice of looking at a 49-yr record with limited depth extent, or a shorter record of one-half of the length but with better depth coverage; we chose the former. Archived data used were corrected for fall-rate errors (Hanawa et al., 1995) for XBTs. Further details on the subsurface temperature data can be found in the appendix. An attempt to assimilate subsurface temperature (and recent altimeter) data by Carton et al. (2000) has produced monthly subsurface temperature estimates for the period 1950–2002 (see online at http://iridl.ldeo.columbia.edu/SOURCES/.UMD/.Carton/.goa/.beta7/.), and these assimilated data have been used by Ruiz-Barradas et al. (2000) for examination of upper-ocean temperature changes correlated with their ''interhemispheric'' mode.
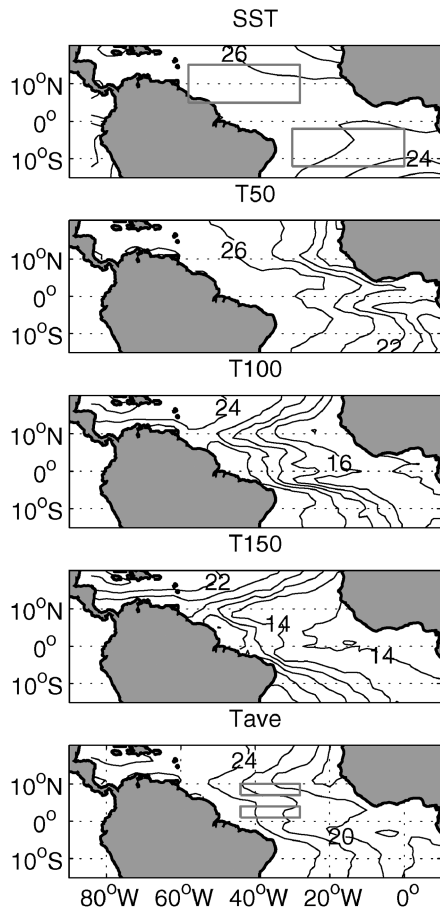
FIG. 1. Mean temperature properties at the surface and at 50, 100, and 150 m and the average between the surface and 150 m are shown for the period 1950–98. All contour intervals are 2°C. Various boxes used later are plotted on the figures. The SST boxes have corners at 5°N, 50°W; 15°N, 30°W; 12°S, 30°W; and 3°S, 5°W.

reported by Clarke and Lebedev (1997) for zonal stress in Comprehensive Ocean–Atmosphere Data Set (COADS). We thus used these NCEP products without correction for time-dependent biases in our analysis. The SST we use is a blended, monthly SST data product (e.g., Reynolds and Smith 1994).

Last, we employ the yearly averaged output of a 40-yr, realistic simulation of the global ocean circulation in the tropical Atlantic from the NCOM. NCOM is a z-coordinate, coarse-resolution global ocean GCM developed for climate studies and has been run in hindcast mode at NCAR. The spatial resolution of the ×2′ version of NCOM is 0.6° latitude at the equator, increasing to 1.2° poleward of 30°, and 2.4° longitude. There are 45 vertical levels, spaced at 8 m near the surface increasing to 258 m at depth. The model is based on the Geophysical Fluid Dynamics Laboratory Modular Ocean Model, version 1.1, and many modifications have been made to converge on more realistic physics (Gent and McWilliams 1990; Gent et al. 1995, 1998; Large and Gent 1999; Large et al. 2001; Doney et al. 2003). To spin up, the model was forced for 333 yr on a coarser grid (the ×3′ version) with initial conditions based on observations. After 5 yr of a single repeat year of forcing, the temperature and salinity fields are interpolated onto the finer ×2′ grid, the velocities are set to zero, and the model is integrated a further 5 yr to allow the velocity field to adjust geostrophically to the density field. The ×2′ model is then integrated with four repeats of the 40-yr NCEP forcing with each run being initialized with the final state of the previous run.

The uncoupled model was driven by net surface fluxes of momentum, heat, and freshwater calculated using the bulk formulas of Large et al. (1997) and surface atmospheric variables from the six-hourly NCEP–NCAR reanalysis covering the period 1958–97. Satellite estimates of cloud fraction, surface insolation, and precipitation were incorporated where available and long-term monthly climatological values were used prior to satellite coverage. Doney et al. (2003) describe the model architecture and forcing and show that the magnitude and phase of interannual variability in the model compare favorably with satellite sea surface temperature and height, and with in situ sea surface temperature and salinity. Capotondi and Alexander (2001) showed that the model reproduces well the enhanced variability at 10°–15°N in the tropical North Pacific, allowing a demonstration that this variability is associated with vertical displacements of the thermocline due to westward-propagating baroclinic Rossby waves with periods longer than 7 yr. Phillips and Joyce (2003, unpublished manuscript) compared the NCOM hindcast with the Bermuda Station S long-term hydrographic time series and showed that above 500 m the model captures well the observed interannual and longer variability in temperature and salinity.

Each of the various data/model products has a different spatial resolution, and we have resorted to resam-

They find subsurface temperatures changing in concert with the SST whereas we will show the opposite. One assimilation product is the heat content in the upper 125 m, which being close to our estimate (150 m), provides a benchmark dataset for comparison. We will discuss this dataset later. Generally, we find that in some regions our data "agree" better with the assimilated dataset than the hindcast model (below), while in other regions, our subsurface heat content follows the hindcast model better than does the assimilated product. Of course, in such an effort, one cannot say in advance, who is "correct."

In addition to the subsurface observations, we use the NCEP–NCAR reanalysis (Kalnay et al. 1996) for monthly surface wind stress. Analysis of errors and bias in the NCEP wind and wind stress was studied by Smith et al. (2001), and generally indicate that wind speeds and stress are underestimated during the World Ocean Circulation Experiment (WOCE) period (1990s) with a slight low bias of around 10% in the Tropics. Neither the meridional nor the zonal wind stress in our equatorial "box" (defined later) exhibited any long-term trend, as

pling to a regular grid of 1° lat × 2° lon in the tropical Atlantic domain between 15°S and 20°N. Our time period of study is a function of the "data" set being used: it can range from 1950–98 for the NCEP/SST products and the SST/subsurface temperature data (49-yr span) to a 40-yr time span, 1958–97, for the numerical model output.

Because of the importance of cross-equatorial winds to tropical Atlantic climate variability, we next examine some interannual relationships of this atmospheric component with other variables such as SST, heat content, and wind stress curl. Since a correlation does not provide any causal relationship, we then look at monthly data and lag/lead relationships.

3. Interannual variability and cross-equatorial wind stress

Because the cross-equatorial winds are expected to respond to the cross-equatorial SST gradients, we first examine the tropic-wide correlation between the time variable meridional winds and other key variables (Fig. 2). We use an index of meridional winds in an equatorial box (see upper panel) and plot the significant correlations with the wind stress curl, SST, and heat content (model and observed). The 95% confidence level for 40 degrees of freedom is ±0.31. We thus show only contours of the cross-correlation coefficient at levels of ±0.3, 0.6, 0.9 in the figure. Any shade of light gray is certainly below the 95% confidence level. White (≥0.3) and dark gray (≤−0.3) shades are likely to be significant. We see that meridional wind stress is significantly anticorrelated with wind stress curl in a zonal band within the deep Tropics. The sense of the correlation is what is expected from the modeling and composite work of Moura and Shukla (1981) and Nobre and Shukla (1996), respectively: as wind blows northward across the equator, it develops a clockwise rotation, with a counterclockwise rotation for wind blowing to the south across the equator. In this analysis we use the oceanographic convention for winds and wind stress. Significant SST correlations are also apparent in regions away from the equator with opposite sign on either side. The sense of the correlation is that positive (northward) winds blow from the cold to the warm hemisphere, also expected from the above-cited work. The lower two panels show much weaker correlations with observed and modeled heat content: clearly the SST signal is more correlated with cross-equatorial winds than the upper-ocean heat content. We will attempt to explain why this is so later. Two off-equatorial boxes have been selected, based on the SST correlation, which will also serve as indices of covariability (indicated in the SST panel of Fig. 2). These will be used subsequently. It is clear that the meridonal decorrelation scale for the meridional winds is greater than for the wind stress curl, the latter is coherent with the winds over a rather limited meridional extent between about ±6°. We have used annually av-
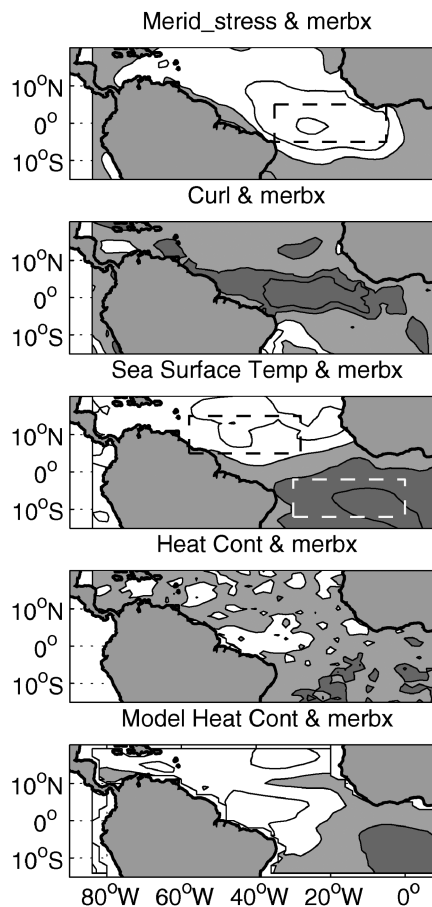

FIG. 2. For the period 1958–97, the correlation coefficient for yearly averaged properties is presented. In each case the meridional wind stress in an equatorial box (merbx) is correlated with meridional stress, wind stress curl, SST, observed heat content (average temperature 0:150 m), and model heat content at each grid point. The contour interval is 0.3 starting from a min of −0.9 and reaching a max of 0.9. Light gray is between −0.3 and 0.3 and is estimated to be below the 95% confidence level. White areas are positive (>0.3) and dark areas are negative (<−0.3). Various boxes used later are plotted on the figures. The SST boxes have corners at 5°N, 58°W; 15°N, 28°W; 12°S, 30°W; and 2°S, 0°. The meridional wind box on the equator has bounds of 5°S, 35°W; 5°N, 5°E.

eraged properties for the above analysis. As pointed out by Frankignoul and Hasselmann (1977), unlagged correlations do not distinguish between cause/effect relationships, for which lagged correlations based on monthly data are more appropriate (see also Frankignoul 1999).

4. SST dipole index and monthly stress anomalies

Using the pair of off-equatorial SST boxes, we have examined monthly NCEP data for a 49-yr period and correlated SST and zonal wind stress anomalies in each of the two off-equatorial boxes. If the zonal wind stress (which is negative in the mean for both regions) becomes more negative (negative anomaly) in these trade
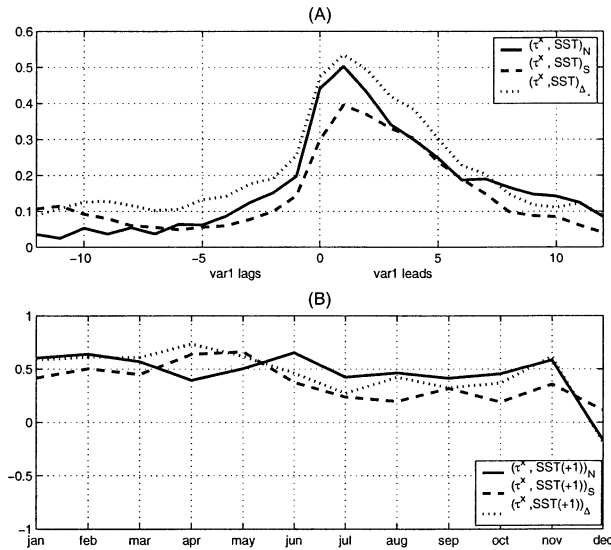
FIG. 3. (a) Monthly cross correlation between zonal wind stress and SST for the northern (solid lines) and southern (dashed lines) SST boxes and their SST/wind stress differences (dotted lines) shown for various lags/leads. (b) The lagged (SST lagged by one month) cross correlation is shown for various months throughout the year for the 49-yr record. Taking into account the autocorrelation properties of the individual time series, we estimate the 95% confidence level for zero correlation to be 0.14.
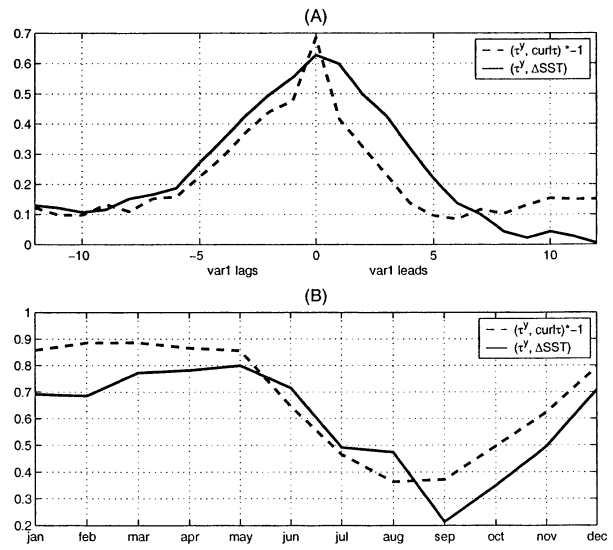

FIG. 4. Similar to Fig. 3 but for (a) the meridional wind stress correlated with the north/south SST difference (solid line) and the equatorial wind stress curl (dashed) in the equatorial box. (b) Unlagged cross correlation for various months of the calendar year. Again, taking into account the autocorrelation properties of the individual time series, we estimate the 95% confidence level for 0 correlation to be 0.16.

wind boxes, the magnitude of the zonal wind stress is increased. As expected from the heat balance in these regions (e.g., Carton et al. 1996) an increased wind speed leads to an enhanced evaporative cooling and hence a lower SST. The sense of the correlation (Fig. 3a) certainly supports this interpretation, with the SST lagging the wind stress anomaly by about a month. Correlations are higher in the Northern Hemisphere box, but highest when the meridional differences in SSTs and stresses are correlated. Were the SSTs and stresses uncorrelated in the two off-equatorial boxes, the correlation coefficient of the differences would be the average of the two individual boxes. Since it is, in fact, larger than either individual correlation leads us to conclude that the two regions are weakly anticorrelated. The index defined by the SST difference is very similar to that used by Servain (1991) and follows that dipole index over the time of overlap. However, our choice of "boxes" for the off-equatorial regions is dictated by the desire to maximize the correlated signal between SST and the meridional wind stress (Fig. 2), which leads us to somewhat smaller spatial regions than used by Servain (1991). Within these boxes, SST is seen to be following zonal stress, in keeping with the idea that the latter drives the former. The one-month lag correlation is mostly independent of month through the year. We have computed this using all of the May stresses (for example) and the June SSTs, and so on for every month of the year (Fig. 3b) with no indication of seasonality. Although the cross correlation is small for SST leading zonal stress, values are marginally larger than the ex-

pected level for zero correlation (especially for the northern box), suggesting some possible, though weak, positive feedback at this off-equatorial latitude.

Contrasting with this is the comparison between monthly anomalies of the meridional stress and curl in the equatorial box and the cross-equatorial SST difference between the northern and southern boxes (Fig. 4a). Here we see the maximum correlation of the meridional wind stress both the ΔSST and $-\mathrm{curl}\tau$ at zero lag. The cross correlation is still highly significant when ΔSST leads or lags the meridional winds by a month or two. There is a strong seasonality (Fig. 4b) with highest covariability in the first half of the year. During this period, the seasonal meridional winds are weaker (they are always positive in a mean monthly climatology of the whole period studied), and the ITCZ is closer to the equator in the first half of the year than in the latter half. This sensitivity of tropical winds to SST signals was noted by Philander (1989, p. 48) who stated, "Apparently sea surface temperature variations in the tropical Atlantic have a much stronger influence on convective zones, especially the ITCZ, during the first half of the year than later in the year."

The seasonal sensitivity and the lag/lead relationship of the equatorial region contrasts sharply with the off-equatorial regions where zonal winds clearly lead SST and there is no obvious seasonality in the effectiveness of the SST response. It seems that the two quantities (meridional winds on the equator and zonal winds substantially off the equator) are not behaving in lock step with one another with respect to the large-scale, cross-

equatorial SST signal. It is common (e.g., Chang et al. 2001) to lump these signals together in examining a leading "mode" of covariability in the tropical winds and SST, even with monthly resolution in time. This may confuse the issue between an SST response that is clearly lagging the zonal winds yet is in phase with cross-equatorial winds. Indeed, it is only in the deep Tropics, within $\pm 10°$ of the equator, where the positive WES feedback may be operating (Czaja et al. 2002; Kushnir et al. 2002). At latitudes of the SST boxes, it appears to be weak.

We have also examined the relationship of the zonal stress in the equatorial box with the SST in the equatorial box, and while SST lags zonal winds by a month, consistent with winds forcing SST, the correlation is weak (0.37) suggesting that other processes are more competitive in setting SST on the equator. Furthermore, zonal winds on the equator are only marginally (-0.32) correlated with the ΔSST, giving a weak westward wind stress while the meridional wind stress at the equator is northward. So while zonal equatorial winds may be thought to drive a different "mode" of variability (Atlantic Niño) that we have not examined, there remains a weak, unexplored relationship with the meridional winds and ΔSST that are the focus of our study.

In keeping with the above, we see the deep Tropics as one region where the positive WES feedback may be working (though most effectively in the boreal winter and spring), and that one prominent consequence of cross-equatorial winds is a zonally extended but meridionally limited region in which the zonal wind anomalies turn as they cross the equator, producing a strongly covarying wind stress curl. This latter quantity can easily produce time-varying, cross-equatorial flow in the ocean, to which we will now turn.

5. Cross-equatorial Sverdrup flow

Using annually averaged quantities, the wind stress curl averaged over $\pm 4°$ of the equator and between longitude bounds of 5°E and 42°W can be used to compute a zonally integrated, wind-driven cross-equatorial Sverdrup transport (Joyce 1988), which we anticipate will be opposite to the cross-equatorial flow in the overlying atmosphere because of the nature of the curvature of the winds crossing the equator. The zonally integrated Sverdrup transport (Fig. 5a) is large and negative. Joyce (1988) used a different wind estimate (Hellerman and Rosenstein 1983) from an earlier epoch and cited a climatological value of -10 Sv (1 Sv $\equiv 10^6$ m^3 s^{-1}), which is like that shown. This mean transport reflects the fact that the NECC, which separates the two counterrotating tropical wind-driven gyres, is located north of the equator. The wind-driven Sverdrup transport is supplied/absorbed by zonal flow associated with the NECC in the north and the South Equatorial Current (SEC) in the south. Were we to choose a latitude of 5°N for this presentation, the temporal variability of the meridional
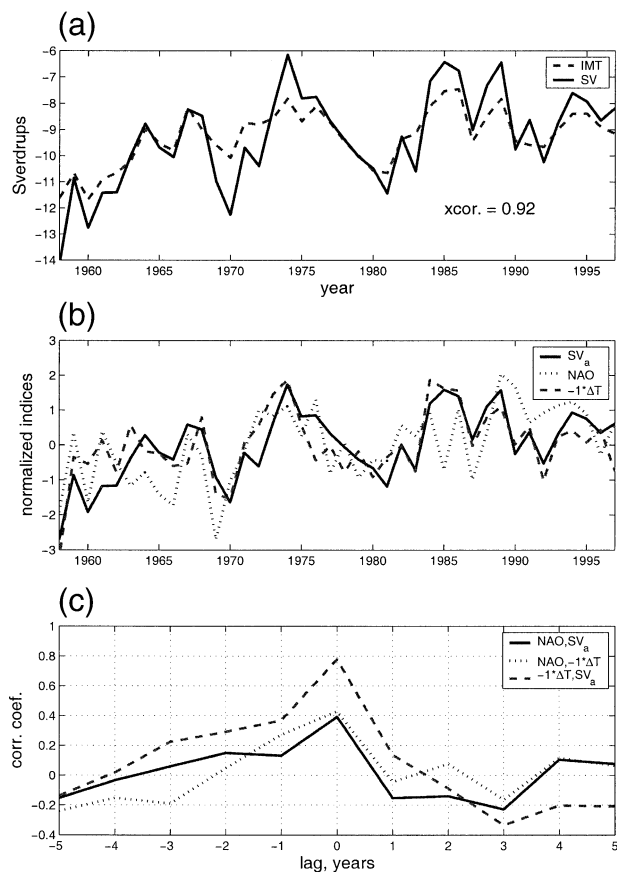

FIG. 5. (a) Cross-equatorial Sverdrup transport as calculated from wind stress curl data (solid line), and interior volume transport from NCOM (dashed). (b) Normalized variables (means subtracted, divided by their respective standard deviations) plotted vs time for the Sverdrup transport (solid), large-scale SST dipole (reversed sign, dashed), and NAO (dotted). (c) Cross correlation of these three variables (detrended).

flow would have been the same, but the mean value closer to zero. It is the variability that interests us here, but we hasten to point out that the NCOM model, which is forced by the same winds that go into our Sverdrup calculation, has similar mean values and variability (cross correlation = 0.92) to the cross-equatorial Sverdrup flow. The model transport has been calculated from the surface down to a mean potential density of 26.6 sigma-theta (approximately 210 m on the equator) and represents the interior regime, isolated from a region of strong northerly flow next to the western boundary. In the model this northward, wind-driven flow on the western boundary extends eastward into the interior to about 31°W, and this western boundary region contains most of the thermohaline, interhemispheric flow as well.

Comparison of the Sverdrup wind-driven flow and the ΔSST signal shows very substantial correlation ($\sim$0.8; Figs. 5b,c). Here and in all subsequent cross correlations, we have removed the mean and any linear trend in the time series prior to cross correlating in order

to focus on the decadal signals not the trends. We have also compared the two series with that of the North Atlantic Oscillation, using an index from Joyce et al. (2000). While some significant, remote influence of the NAO is reflected in the analysis, it is substantially less than intratropical variables and probably reflects a relatively low impact of NAO variability on the SST and wind fields of the Tropics.

The cross-equatorial transport variability is of order 1–2 Sv, with a mean of −10, or about 10%–20% of the mean. With the direction of the anomalous oceanic flow opposite to that in the atmosphere, water is transported across the equator from the warm side to the cold side of the SST gradient. This represents a transfer between the two counterrotating tropical gyres whose separatrix is the NECC, at ~5°N. While we have not shown that the variability of the wind stress curl at the equator is essentially unchanged from that at 5°N, one can see this indirectly by examining the structure of the spatial correlation between the wind stress curl and the meridional wind stress in the equatorial box (see Fig. 2b). Since the time-varying Sverdrup transport is always from the warm to the cold hemisphere (in terms of SST), it must act to reduce the gradient of the dipole.

6. A 1.5-layer model for the dipole-induced, wind-driven flow

In order to illustrate the oceanic response to the dipole-induced wind stress forcing, we have done some numerical calculations with a linear 1.5-layer reduced-gravity model. This model has one active layer, which is driven by the surface wind stress. The model is governed by the following equations:

$$\frac{\partial u}{\partial t} - fv = -g'\frac{\partial h}{\partial x} + A_H\left(\frac{\partial^2 u}{\partial x^2} + \frac{\partial^2 u}{\partial y^2}\right), \quad (1)$$

$$\frac{\partial v}{\partial t} + fu = -g'\frac{\partial h}{\partial y} + A_H\left(\frac{\partial^2 v}{\partial x^2} + \frac{\partial^2 v}{\partial y^2}\right), \quad (2)$$

and

$$\frac{\partial h}{\partial t} + H\left(\frac{\partial u}{\partial x} + \frac{\partial v}{\partial y}\right) = 0, \quad (3)$$

where $\mathbf{u} = (u, v)$ is the velocity, $A_H = 10^3$ m^2 s^{-1} is the viscosity, h and H are anomalous and mean layer thickness, and ρ is the water density. The mean layer thickness H is set to be 200 m in all experiments. The value of the reduced gravity g' is chosen so that the gravity wave speed $c_p = \sqrt{g'H}$ is 2.4 m s^{-1} (corresponding to the first baroclinic mode in the tropical ocean). The Rossby deformation radius $R = \sqrt{c_p/2\beta}$ is about 230 km. The model extends from 25°S to 25°N meridionally and 40° zonally. The model resolution is 1/4° in both zonal and meridional directions and it resolves all first baroclinic mode equatorial waves. The western and eastern boundaries are solid walls at which no-normal-flow and no-slip conditions are applied. The

northern and southern boundaries are open so that signals can exit freely from the model domain.

As discussed earlier, the dipole-induced, time-dependent wind tends to blow from the cold to the warm hemisphere. As these wind anomalies cross the equator, the northward wind tends to rotate clockwise and thus the wind stress curl is negative, and vice versa for the southward wind. This wind stress pattern is limited to the deep Tropics. We create a model wind field that mimics the dipole-induced wind pattern for the first numerical calculation:

$$\tau^y = \tau_0(t)e^{-(x-x_0)^2/X^2 - y^2/Y^2}, \quad \text{and} \quad (4)$$

$$\tau^x = -c_0\partial\tau^y/\partial y, \quad (5)$$

where $x_0 = 20°$, $X = 10°$, $Y = \sqrt{50°}$, and c_0 is an algebraic constant. The wind field and its curl are shown in the upper-left panel of Fig. 6. This clearly resembles the wind induced by a SST dipole with warm anomaly in the Northern Hemisphere. The model is then forced by the wind stress that varies sinusoidally for a period of 10 yr, that is, $(\tau^x, \tau^y) \sin(2\pi t/T)$ (where $T = 10$ yr), and is chosen to have a similar magnitude to what is observed.

The anomalous layer thickness h and velocity field at $t = 12.5, 15, 17.5,$ and 20 yr are shown in the lower-left column of Fig. 6. At $t = 12.5$, the wind stress curl is at the peak of the negative phase, and thus the southward Sverdrup transport is maximum. This has produced a dipole structure of thermocline depth across the equator, with a shallow upper layer on the warm side of the SST dipole. A northward western boundary current is present to balance the southward transport in the interior. There are two important time scales here: one is the 10-yr period imposed in the wind field, and the other is the oceanic adjustment time scale. Since the forcing is antisymmetrical about the equator, only even-numbered meridional mode Rossby waves are excited (inertial gravity waves and Yanai waves are absent because of the low-frequency forcing). The fastest wave is the second meridional mode Rossby wave, which travels westward at 1/5th of the gravity wave speed: $\simeq$0.5 m s^{-1}. It takes about 1.7 months for a Rossby wave at the center of the basin to reach the western boundary and to set up the boundary current. This time scale is much shorter than the imposed 10-yr period. So the oceanic response is nearly instantaneous to the forcing field and is nearly in phase with the varying wind field. The magnitude of interior transport across the equator (excluding the western boundary current) is 2.0 Sv, while the magnitude (1.9 Sv) of the zonally integrated Sverdrup transport, v = curlτ/β, matches well the model simulation. All the interior transport is balanced almost exactly by the opposite transport at the western boundary, and so the net cross-equatorial transport is near 0.

In the second experiment, we use only the meridional wind stress, $(0, \tau^y)$, to force the model. The curl is very weak and changes signs across $x = 20°$, as shown in
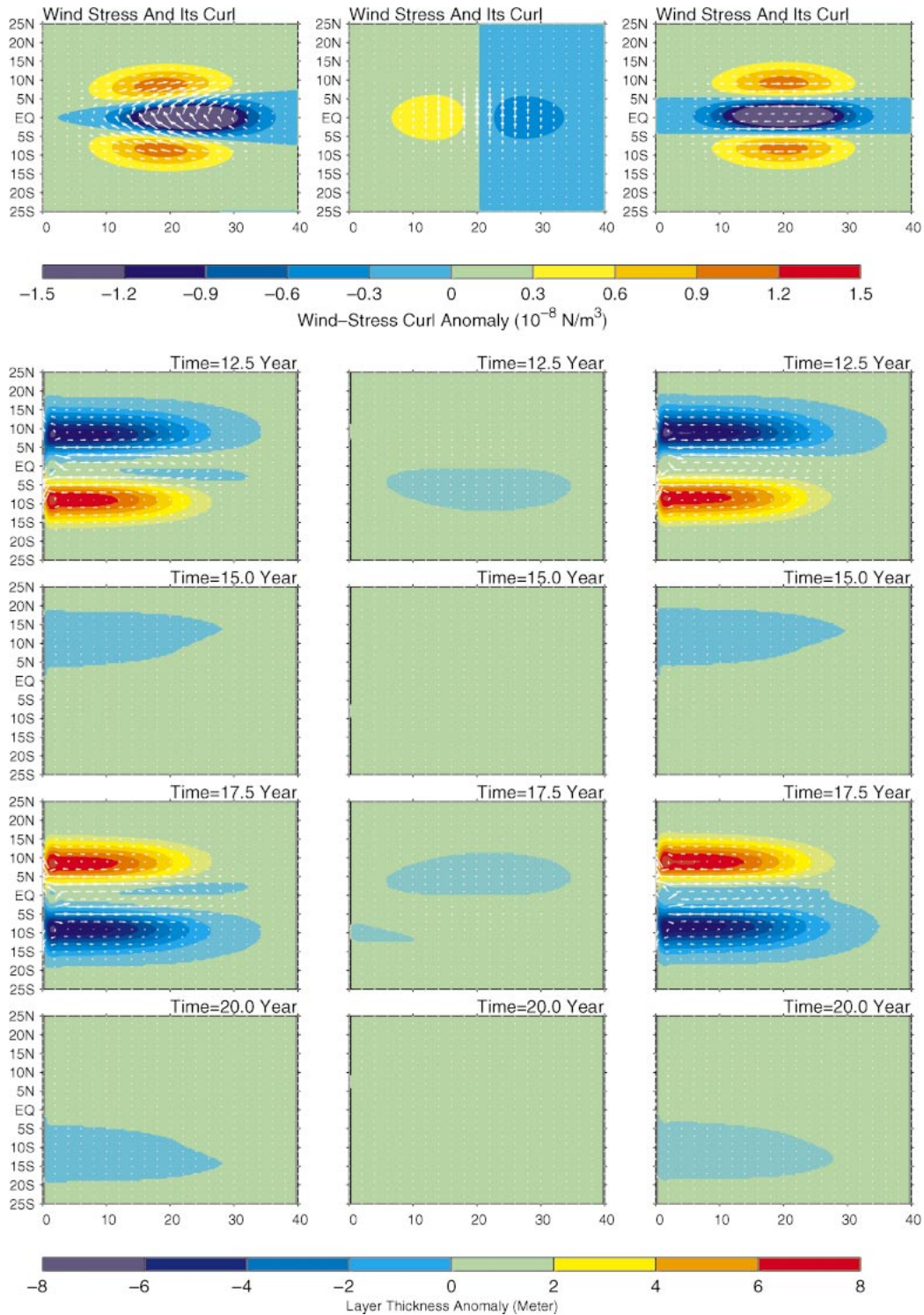
FIG. 6. (top) Reduced-gravity model of an idealized tropical Atlantic with wind stresses that (top left) mimic the observed structure, (top middle) contain only meridional winds, and (top right) contain only zonal winds. In all cases the wind forcing is varied sinusoidally with a 10-yr period. (bottom) The upper-layer thickness (contours) and current velocities (arrows) for the second cycle: (second row) 12.5, (third row) 15, (fourth row) 17.5, and (bottom) 20 yr.

the middle of the top panel in Fig. 6. There is an interior cross-equatorial transport in the western half of the basin and an equal and opposite one in the eastern half. These compare well to the expected Sverdrup transports but result in a negligible, net cross-equatorial transport.

In the next experiment, only the zonal wind stress, $(\tau^x, 0)$, is used. The magnitude of the wind stress curl is nearly as great as in the first experiment. The model result is also almost identical to the first one, indicating that it is the off-equatorial turning of the meridional wind into the zonal direction thus producing a curl of the wind stress, and not the meridional stress itself that is key to the oceanic response.

Last, we note that the thermocline depth variation of the model is approximately ± 6 m, with dipole-like structure that is such as to have a shallow (deep) thermocline on the side of the basin toward (from) which the meridional winds are blowing. The model is trying to reproduce the wind-driven effect of the SST dipole and since the meridional winds blow from the cold to warm side of the equator based on SST, the model suggests a shallow thermocline on the warm side of the equator and a deep thermocline on the cold side. Although our 1.5-layer model presently contains no thermodynamics, it seems likely that the wind-driven ocean response might produce a negative feedback on SST based on thermocline depth changes. This will be explored in a different context below, but first we turn to a manifestation of the cross-equatorial, wind-driven flow, which can be estimated from data.

7. Interannual transport of the NECC

One feature of the mean wind-driven flow in the tropical Atlantic is the generation of substantial zonal flows off the equator that feed the interior from the western boundary. In the Southern Hemisphere this is the SEC and to the north, the NECC. Because of the greater data density to the north, it is here that we have some hope of verifying the ocean response to the dipole through comparisons between the zonal Sverdrup flow of the NECC with subsurface ocean observation of geostrophic zonal flows in the region of the NECC. First, consider the Sverdrup flow in the NECC, which can be estimated by integrating the meridional transports at two latitudes spanning the NECC from the eastern boundary to near the western boundary. We chose to average the wind stress curl between $1°$ and $4°$N for the southern limit and between $7°$ and $10°$N to the north, giving estimates of the zonal Sverdrup transport at $42°$W by taking the divergence of the two meridional transports. The eastern boundary was fixed to be $15°$E at the southern limit and the Greenwich meridian at the northern limit. Geostrophic, zonal transports are estimated in a two-step process. First, we estimate the mean, vertically averaged temperature difference across this latitude span from the oceanic data, averaged in two small boxes shown in the lower panel of Fig. 1. These extend zonally between

$44°$ and $20°$W and are chosen to increase our signal to noise ratio in the hydrography. The gridded, subsurface data are gappy in space and time and a greater averaging area increases the signal while the near zonally uniform flow remains fairly constant over this zonal extent: mean temperature contrasts remain fairly constant at about $2°$C over this range of longitudes (Fig. 1e). This mean temperature difference, gives an estimate of the dynamic height difference and thus the vertical geostrophic shear. The mean Sverdrup transport across the NECC (10.7 Sv) is then used to "scale" the mean temperature difference (2.2°C), calculated as the difference between the southern and northern limits of the NECC. In step two, this mean scaling between the mean temperature (or heat content) of the upper 150 m, and the mean zonal Sverdrup transport is used to infer what we expect for transport *variability* from the temperature data. In effect, we are assuming that the vertical structure of the variability will be similar to that of the mean flow and that temperature/salinity (T/S) variability is comparable to the T/S structure of the mean fields. After detrending the data, results (Fig. 7b) represent the time-variable transport of the NECC between latitudes of $2.5°$ and $8.5°$N.

Next, the mean temperature difference (again south minus north for the small NECC boxes) is cross correlated with both the large-scale temperature gradient index for the dipole used previously (Fig. 7a) and the zonal transport of the NECC (Fig. 7c). We discuss first the two transport estimates, followed by the two temperature estimates.

While the covariability of the two zonal transport time series is significant, it is not large (cross correlation $\sim$ 0.44). Given the uncertainty in the oceanic data, however, it is strongly suggestive of a covarying signal. In an examination of inverted echo sounder measurements across the NECC (Katz 1993) for the period of 1983 to 1989, interannual dynamic height differences between $3°$ and $9°$N of amplitude ± 8 cm (relative to 500 dbar) were estimated from moored observations spanning the NECC at $38°$W. The range of variability was small compared to the annual signal (30 cm), illustrating one problem we (not Katz) have with our approach, which only partially compensates for the annual temperature signal. Nevertheless, the Katz results showed high NECC transport in 1983 and 1987, in good agreement with our results. His attempt to use a numerical model to explain the variability in terms of wind-driven flow was unsuccessful, however. Furthermore, no attempt was made (or at least published) by Katz to compare the observed interannual transport variability of the NECC with that expected by the Sverdrup transport. In contrast to Katz's model results, the NCOM model shows a high degree of correlation between the zonal transport variability of the NECC and the expected Sverdrup transport (Fig. 7c), although the rms amplitude of the model NECC variability is only about one-half that of the zonal Sverdrup transport (not shown). This is due to the model NECC being spread over a wider latitude range ($3°$–
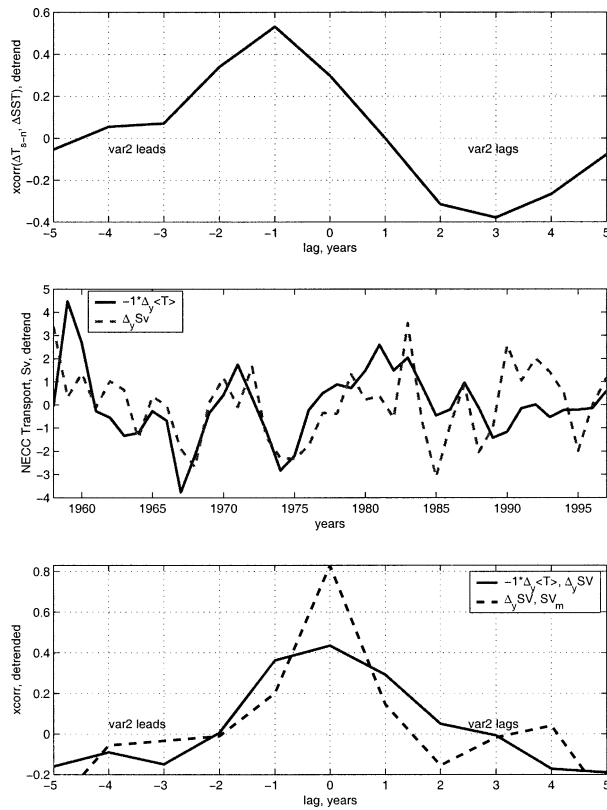
FIG. 7. (top) Mean temperature difference between two small boxes (shown in Fig. 1, south minus north) bounding the NECC and the large-scale dipole SST signal (north minus south) have been cross correlated and detrended. (middle) The ocean temperature data have been scaled (see text) to be the time-varying geostrophic transport of the NECC (solid line) and compared with the zonal flow expected from the Sverdrup balance between 2.5° and 8.5°N (dashed). (bottom) The cross correlation of the zonal Sverdrup transport with the transport estimates based on upper-ocean temperature and NCOM output, all detrended.

11°N) than the bounds chosen for our analysis. The limited time period studied by Katz was not one of substantial variability over the 40-yr record, in which we observe, or at least infer, decadal variations of the NECC transport having an amplitude of 2 Sv, approximately 20% of the mean. The Carton et al. (2000) assimilation product of heat content in the upper 125 m was also examined for the NECC transport. Since this product is given with monthly resolution, its annual mean should not suffer from the sort of sampling biases we tried to circumvent in our own subsurface analysis. Yet the correlation between the assimilated heat content difference between the two regions used for the NECC analysis and the wind-driven Sverdrup flow was only slightly greater than for our subsurface analysis (0.46 as compared with 0.44), while the correlation between the two subsurface datasets, while greater than their correlation with NCOM, was still relatively low (0.4).

Based on our yearly mean analysis, the geostrophic signal lags are about 0.5–1.5 yr behind the dipole (Fig.

7a) suggesting that the NECC is not in phase with the large-scale forcing. This may be surprising since the variance in the Sverdrup transport near the equator (2.5°N) exceeds that at 8.5°N by more than a factor of 8, and we have already shown that cross-equatorial Sverdrup transport variability is in phase with the wind stress curl (and the dipole index) with no lag. However, the inclusion of off-equatorial winds at 8.5°N, while small in variability of the curl as compared with those near the equator, has introduced some subtle lag into our analysis, possibly related to local mass accumulation in the region of the NECC. A similar approach to estimating the variable NECC transport in the western Pacific Ocean (Qiu and Joyce 1992) using hydrographic data at 137°E and comparing the variability to the expected Sverdrup transport, showed no time lag between the geostrophic transport and the wind driving. At the time we did that calculation, there was little hope of explaining *any* simple linear response of the Pacific in terms of wind driving, yet it clearly emerged. What we find in the tropical Atlantic is an encouraging yet not completely conclusive indication that linear dynamics governs the variability in the NECC. One would expect that this signal would be measurable in the PIRATA array (Servain et al. 2003) once a sufficiently long enough record is obtained from the moorings spanning the NECC.

8. Oceanic feedback on the SST dipole

Our reduced-gravity model indicated that meridional, wind-driven flows will act to transfer heat anomalies across the equator and ultimately change the volumes of the reservoirs on either side of the equator: reducing (increasing) the reservoir thickness or heat content on the warm (cold) side of the SST dipole. Because the time lag between the forcing and the wind-driven response is fast, there is no decadal "oscillation" that can develop: the ocean response is nearly in phase with the forcing and acts to reduce the heat content/SST signal created initially by the atmosphere. Hence, it is not surprising that SST may strongly covary with wind driving, but heat content may not, in agreement with our earlier results (cf. Figs. 2c and 2d,e). We expect the SST signal that initiates this flow will be damped by the ocean response. The question is whether this is significant enough to need to be considered in climate variability of the Tropics. We now seek to evaluate the degree of damping using the observations already presented. We develop two different models, similar in that they both contain a negative ocean feedback, but different in the parameterization.

a. Linear feedback model

Because of its fast adjustment, the tropical atmosphere reacts nearly instantaneously to changes in the meridional SST gradient. Near the equator, the oceanic

Sverdrup transport responds on time scales of days (barotropic) to months (baroclinic) to the changes in the wind stress curl, so that with yearly data only a very small delay is expected between ΔSST (denoted here by ΔT) and the resulting Sverdrup transport at the equator (denoted by q). To a good approximation, we can thus set

$$q(t) = -b\Delta T(t) + \text{noise}, \qquad (6)$$

where the minus sign recalls that a positive SST gradient generates a negative (southward) Sverdrup flow. To estimate b from the Sverdrup transport and SST data, we use regression analysis, assuming that ΔT is the independent variable (all the noise is in q, as the ocean also responds to unrelated atmospheric variability). The correlation in (6) is highly significant (-0.78), yielding $b = 6.6$ Sv K^{-1}. Consistent with our assumption of a fast response, the correlation is negligible (-0.14) when q leads by 1 yr, and of small magnitude (-0.37) when q lags by 1 yr. Note that such slight asymmetry is consistent with ΔT driving the oceanic response, while no asymmetry would be expected if the atmosphere was driving both ΔT and q (alternative null hypothesis).

Since the SST is warmest on the average along the mean position of the ITCZ, north of the equator, an increase in (northward) Sverdrup transport should increase ΔT, as it would bring warmer water to the north and colder to the south. If the changes in Sverdrup transport are resulting from the wind stress curl response to the cross-equatorial SST gradients, their latitudinal extent should be limited to the deep Tropics (see Fig. 2b), thus only partly overlapping with the two off-equatorial boxes that define ΔT. As the mean near-surface circulation due to the trade winds contributes to poleward advection, however, the increase in SST gradient should be spreading poleward, so that the maximum impact on ΔT occurs after a delay. Using 1 cm s^{-1} as an order of magnitude for the meridional currents suggests a delay of about a year, consistent with the higher correlation that is found between $\partial_t\Delta T$ and q when the latter leads the former by 1 yr (0.50) than when they are in phase (0.33) (Fig. 8).

To model this process, one cannot simply assume that $\partial_t\Delta T$ is proportional to $q(t - 1)$, where t is in years, since the SST dipole is itself primarily driven by local atmospheric forcing, as argued above. We thus add our ocean circulation feedback to the simplest model for atmospherically driven SST, the first-order Markov process of Frankignoul and Hasselmann (1977),

$$\partial_t\Delta T(t) = f(t) - \lambda\Delta T(t) + aq(t - 1). \qquad (7)$$

Here $f(t)$ represents the difference in stochastic atmospheric forcing between the two boxes, and for simplicity we have assumed that the same damping term was acting on the two SST boxes. Both atmospheric and oceanic processes may contribute to the damping. The influence of mixing processes in the ocean is difficult to estimate, but Frankignoul et al. (2004) have argued
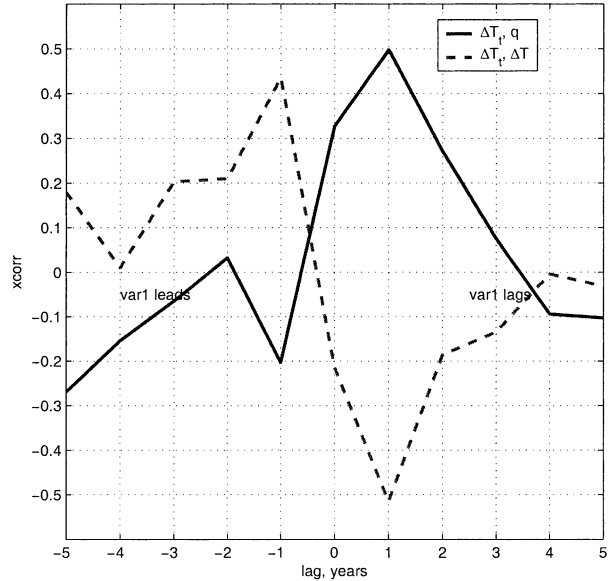

FIG. 8. The correlation between the rate of change of SST difference and both the interior Sverdrup transport (solid line) and SST difference (dashed line). The latter shows the expected antisymmetry but deviations from this are due to the effect of oceanic damping. Maximum damping occurs with a temporal lag of 1 yr between the ocean advection and the observed SST difference tendency.

that their contribution to λ in the tropical Atlantic was on the order of 1 yr^{-1} at large scales. In this region, the negative heat flux feedback is slightly negative, on the order of 5 W m^{-2} K^{-1}, but it may be "neutral" (no feedback) for the SST anomaly dipole, presumably because of the positive contribution of the WES feedback (Frankignoul and Kestenare 2002). We thus choose $\lambda = 1.5$ yr^{-1} as characteristic value in (7), which is somewhat smaller than the 2 yr^{-1} used by Czaja et al. (2002).

The parameter a in (7) can again be estimated by regression. Because the correlation between $\partial_t\Delta T$ and ΔT is small (-0.2), we use the lag-1 regression between $\partial_t\Delta T$ and q to estimate a, yielding 0.06 K Sv^{-1} yr (no error on q). Replacing in (7) and using (6) then leads to

$$\partial_t\Delta T(t) = f(t) - \lambda\Delta T(t) - c\Delta T(t - 1), \qquad (8)$$

with $c = ab = 0.4$ yr^{-1}, which is of the same order but somewhat smaller than λ. Consistent with (8), the correlation between $\partial_t\Delta T$ and $\Delta T(t - 1)$ is large and negative (-0.51). Note that a negative correlation is also expected from the AR-1 model, that is, from (8) with $c = 0$. However, the latter would lead to a fully antisymmetric behavior at positive and negative lags, whereas the correlation between $\partial_t\Delta T$ and $\Delta T(t + 1)$ is of slightly smaller magnitude (0.43). There is thus a slight negative bias of the estimated cross-correlation function, as expected from our positive estimate for c. We will evaluate this model's statistical behavior below, after we introduce a second model for the ocean feedback.

b. Nonlinear, two-box model

As an additional check on the utility of the interior ocean circulation as an agent for negative feedback, we consider a two-box model of the tropical Atlantic: one box to the north of the equator and a second to the south. Between these two boxes, there is a time-dependent interior transport (with a return flow in the western boundary). This transport q is a linear function of the existing temperature difference between the two boxes, ΔT. If the coefficient of proportionality between the above two variables is $-b$ as before, and the volume of each of the boxes is given by V, then one can write a simple time-dependent expression for the change in the temperature difference as

$$\partial_t \Delta T + 2V^{-1}|q|\Delta T + \lambda \Delta T = f,$$

where

$$\Delta T \equiv T_2 - T_1, \qquad f \equiv f_2 - f_1, \qquad V \equiv Ah, \quad \text{and}$$

$$q = -b\Delta T, \tag{9}$$

where f_j is the stochastic forcing of box j. Note that there is no delay with advection in this model, as opposed to the one above, because the two boxes in this conceptual model are contiguous. The absolute value, $|q|$, appears in (9) because advection always acts to reduce temperature differences between the two boxes. A system in which the WES positive feedback dominates over the negative feedback is one in which $\lambda < 0$. If we look at steady solutions to (9) in which the stochastic forcing, f, vanishes, we see that if λ is positive, there is only one solution, that in which $\Delta T = 0$. This solution is stable in time. In the case in which λ is negative, there are three steady solutions to (9):

$$\Delta T = 0, \ \pm\lambda V/2b. \tag{10}$$

The zero solution is unstable, while the two nonzero solutions are stable and reflect the state in which the WES feedback drives a mean temperature difference that is ultimately arrested by the negative, *nonlinear* ocean feedback. If we use WES feedback estimates as in Xie (1999) or Zhou and Carton (1998), and estimates for the relation between the cross-equatorial temperature difference and the shear in the zonal winds from our work or that of Kushnir et al. (2002), we obtain a value for λ of ~ -0.3 yr^{-1}. If advection between the boxes is the only mode of negative feedback, then (10) provides an estimate of the temperature difference of the stable points. With a box thickness of 100 m and a surface area of 4×10^6 km^2, we obtain the following estimates for $(\Delta T, q)$, using (10):

$$\Delta T \approx \pm 0.3 \text{ K} \quad \text{and} \quad q \approx \mp 2 \text{ Sv}, \tag{11}$$

where we have used the same value for b ($=6.6$ Sv K^{-1}) as for the linear model above. These are quite reasonable numbers given the uncertainty of some of the parameters. We conclude that the nonlinear, negative feedback is therefore a possible brake on the positive WES feed-back. In the event that other modes of negative feedback exist, this model provides an additional mechanism that can damp the SST difference.

c. Simulation of time-dependent solution with both models of ocean feedback

We have explored a simulation of the solution of the time-dependent problem with stochastic white noise forcing using a random number generator and a weekly time step. A null model with no time-dependent ocean advection is included for comparison. For the two models with time-dependent ocean advection, we have relaxed the advection to that of the expected Sverdrup response with a short time lag of 2 months. The resulting solutions have been simulated for two cases: one with overall positive, WES-dominated feedback with $\lambda = -0.3$ yr^{-1}, and one with an overall negative feedback with $\lambda = 1.5$ yr^{-1}. In the first example (not shown), we see evidence that the nonlinear model provides sufficient damping so as to give an overall negative feedback equivalent to 0.3 yr^{-1} in the null model, with some evidence of the above stable attractors at nonzero values of the temperature difference. The linear feedback model develops a slight oscillation, due to the stochastic forcing and the delayed negative feedback from the advection. When larger, more realistically positive values of the atmospheric and oceanic damping parameter λ are chosen (1.5 yr^{-1}) all models behave similarly, with variable ocean currents adding a negative feedback to the initial value, increasing the overall negative feedback to that of the null model with an equivalent λ value of 2 yr^{-1}. The resulting autocorrelation functions for SST difference (Fig. 9a) show that both models with advection increase the negative feedback and decrease the time scale for their respective autocorrelation functions from the null model. They are a reasonable approximation to what is observed (Fig. 9b) but with part of the negative feedback now ascribed to the process under study. As to the observations, we also present the autocorrelation structure of the meridional wind stress and wind stress curl from the equatorial box, both of which show a more rapid decay with time than SST difference, yet still have more persistence than winds in the two off-equatorial boxes.

9. Discussion

The connection studied in Fig. 7a involves several steps: SST $\rightarrow$ meridional, cross-equatorial winds $\rightarrow$ cross-equatorial wind stress curl $\rightarrow$ cross-equatorial Sverdrup transport $\rightarrow$ interior response to wind forcing $\rightarrow$ subsurface heat content changes. Somewhere in this chain a time lag has been introduced that, while as yet unexplained but possibly associated with mass storage in the region of the NECC, allows us to suggest that the dipole index can be used as a predictor of changes in the ocean heat content and transport of the NECC.
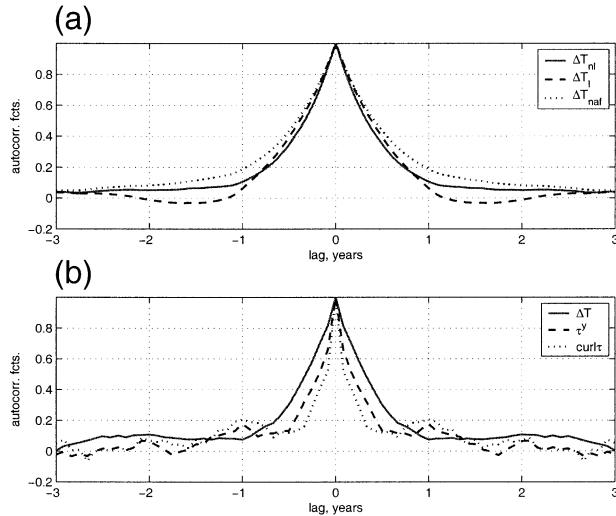
FIG. 9. (a) Three models of SST difference are compared in a simulation of the time-dependent behavior of the forced response of the SST difference in the tropical Atlantic. We consider the case in which the signal is driven by stochastic forcing but no time-dependent ocean advection (null hypothesis; dotted line) with a linear damping coefficient λ of 1.5 yr^{-1}. Both the linear and nonlinear models of ocean damping (dashed and solid lines, respectively) provide additional negative feedback to SST roughly equivalent to the null model with a damping value of 2 yr^{-1}. (b) Using the observed variability meridional SST difference, and for our equatorial box, the meridional wind stress and stress curl, similar autocorrelation functions are estimated and plotted. The SST autocorrelation plot can be compared with those modeled in (2).

One can see directly the effect of cross-equatorial winds on the NECC in the lower panel of Fig. 2, where heat content changes are positively correlated with meridional winds in the western half of the equatorial basin, in the region which forms the southern boundary of the NECC. Northward winds and a strong negative curl cause a downwelling of the thermocline and an increase of the local dynamic height (heat content). To the north of the NECC there is little effect of the winds on heat content. Thus, the zonal transport of the NECC (Fig. 7b) is affected. Outside of this region, with the exception of the South Atlantic, near 10°S, 20°W, there is little effect of the meridional winds on heat content change. We have argued that the wind-driven response of the tropical Atlantic Ocean's thermocline depth is such as to oppose the SST signal, and thus reduce the overall heat content correlation with meridional winds from that expected by SST alone.

The time-dependent exchange of mass between the two counterrotating tropical, wind-driven gyres across both the equator and the mean position of the NECC is an interhemispheric mode of exchange, which has received little attention. The link between the SST dipole and the NECC variability seems well supported by both data and models, and thus the effect of SST on ocean variability in the tropical Atlantic is significant. However, the significance of this mode of variability to the atmosphere as a form of negative feedback on SST is

not as clear. In both the linear and the nonlinear models, we find that under certain conditions of weak damping by other agents (atmospheric feedback or upwelling/entrainment by the ocean), the negative feedback by variable ocean currents can be of the same order as that obtained for midlatitude estimates for the combined effect of mixed layer entrainment, and damping of SST signals by the atmosphere. In the linear model, a lagged negative feedback is suggested; in the nonlinear model, time-dependent ocean flow advects a time-dependent SST signal with little or no time lag. In both cases, the feedback does not itself produce self-sustained oscillations, even given a positive action of the WES feedback, which can locally amplify the signals. Thus, the effect of the ocean feedback alone is not the ultimate cause of tropical Atlantic variability, but is a contributor to its amplitude.
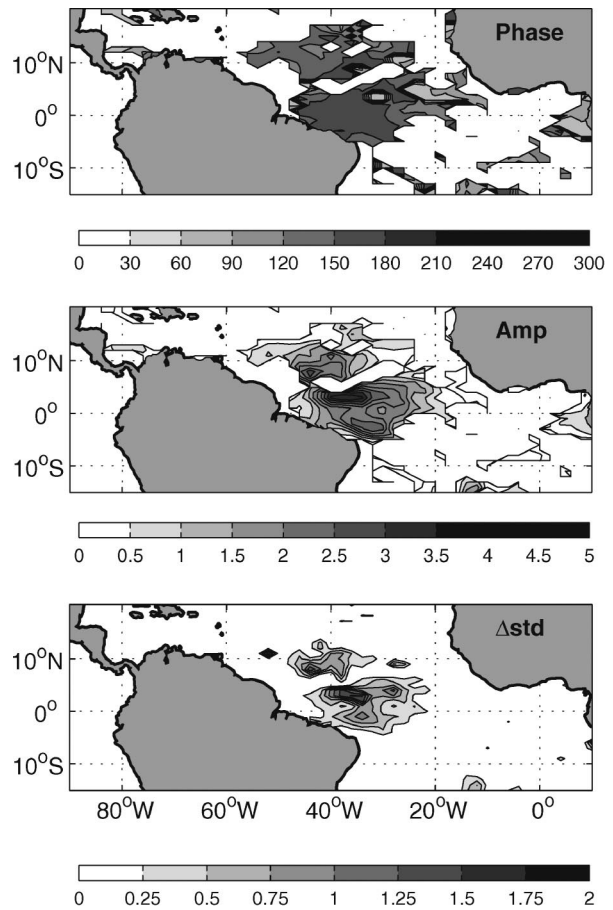
FIG. A1. For the 49-yr time span: 1950–98, the first annual harmonic has been estimated from the subsurface temperature data at 100-m depth. The (top) phase (angular degrees), (middle) amplitude (°C), and (bottom) reduction in interannual temperature signal by removing the seasonal sampling bias (°C) are shown.

APPENDIX

Analysis and Gridding of MBT/XBT Data

Between 1950 and 1998, approximately 158 000 individual data points representing unique measurements of T at 100 m were collected. More data were available at 50 m and fewer at 150 m, with a notable change after 1972 when numbers of data–year at all three depths were practically the same. While impressive in its coverage of the tropical Atlantic, the available MBT and XBT data start to develop large spatial gaps when one looks at them for an individual year. Generally, 2000–4000 points are available in the domain each year with 1974 being a banner year, with almost 12 000 available measurements and 1950, 1951, and 1955 each being years with <1000 samples. Even at present, with quarterly XBT transects of the region, there are still large spatial gaps between sections. For this work, we wanted to obtain good estimates of interannual variability without overly averaging spatially, which would smooth out spa-

tial gradients associated with ocean flows, which can be quite narrow zonally in the Tropics. We chose a 1° lat × 2° lon grid for this purpose and decided not to attempt any temporal resolution better than yearly averages. Because the seasonal signal is quite large in the Atlantic, we needed to address the issue of seasonal bias before calculating annual averages. For example, in one region if most of the annual data were collected in boreal summer during a particular year and during boreal winter in the next year, the annual averaged temperature at depth would be biased high in the first year and low in the second, thus corrupting the interpretation of interannual changes.

After removing outliers from the dataset within one grid point from each of our targeted grid points, data from all years were composited by month and an annual first harmonic was fitted to the seasonal data by least squares. If either the number of data points found within the 1° × 2° box was less than 10 or was greater than 10 but the percent variance explained by the first harmonic was less than 10%, then we did not do any adjustment before binning. If a reasonable seasonal signal could be estimated, then anomalies from the mean seasonal cycle were calculated for each data point before binning.

As an example, we show (Fig. A1) the 100-m depth horizon and the phase and amplitude of the first annual
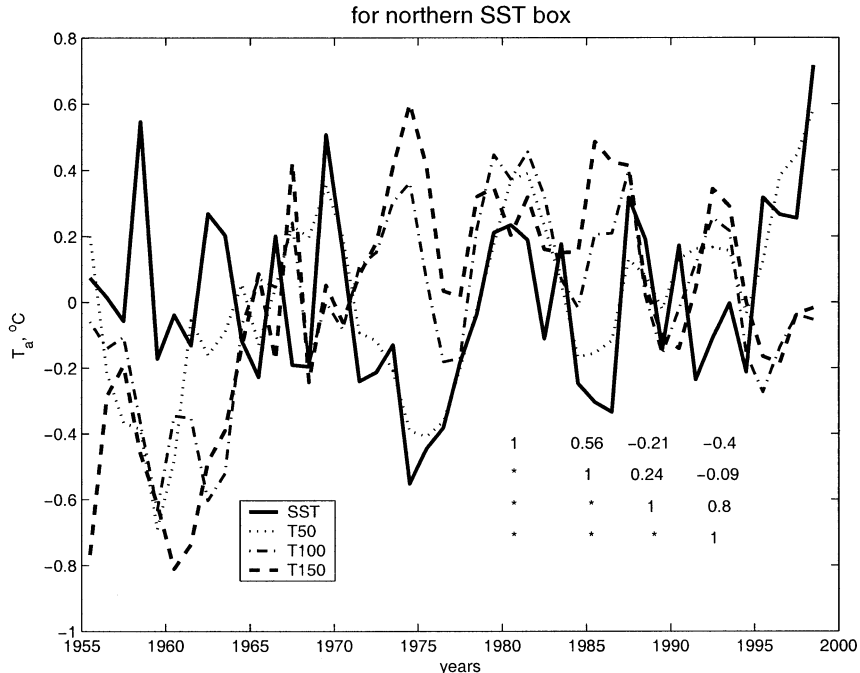

FIG. A2. The northern SST box is defined by lat/lon bounds of 5° and 15°N and 58° and 28°W. In this box we show the annual mean temperatures at the surface, 50-, 100-, and 150-m depth. Subsurface data from MBTs–XBTs have been processed to remove any seasonal sampling bias and show a clear tendency to be opposite in phase from the near surface (0, 50 m) to the deeper (100, 150 m) levels. The inset in the lower right gives the cross-correlation matrix for the four levels, after a linear detrending of the plotted time series.

harmonic (in degrees Celsius and angular degrees). The latter quantity can be interpreted as the yearday on which the temperature achieves its highest seasonal value. After this procedure, we filtered the resulting data using a Laplacian-type filter with a center weight of one-half and one-eighth for the four adjoining cells. This provided a minimal smoothing and extension of gridded data into adjacent, empty cells. We then computed the interannual standard deviation with and without the annual fit and show the reduction of temperature "error" we were able to achieve (Fig. A1, lower panel). In some regions, this amounted to rms temperature corrections in excess of 1°–2°C, but in other areas variance reduction was either small or could not be estimated because of our inability to determine a stable annual signal.

We show (Fig. A2) the surface and subsurface temperatures used in this study for the "northern SST box." This box is one in which SST changes are particularly well coupled to cross-equatorial winds, as discussed in the main part of this report. Heat content variability (not shown) is calculated from the data presented at these discrete depths (0, 50, 100, 150 m). Variability is roughly constant over time, with a suggestion of greater variability at the beginning of the record. Gradual increases in subsurface temperature at 100- and 150-m depth can be seen in the early to mid-1960s. These are not due to changes over from MBTs to XBTs (which occurred in the late 1960s), and observed changes are larger than expected from possible fall-rate errors still not corrected. In fact the latter would produce lower subsurface temperatures at a given depth. As an inset in the figure, we show the cross-correlation matrix for the different levels, after removing linear trends. Overall, SST and T at 50 m variability tracks together without lag, while T at 100 m and T at 150 m tend to follow one another and be antiphase with the near surface. The anticorrelation between SST and T at 150 m (-0.4) is at the 5% significance level and reflects an upward (downward) thermocline displacement under a warm (cold) SST, as previously discussed by Houghton (1991). This relationship is consistent with the dynamics discussed in the main body of this work. Using an assimilation model incorporating subsurface thermal data, Ruiz-Barradas et al. (2000) find SST and upper-ocean temperature in phase near the surface with a suggestion of out of phase behavior below 100 m in midbasin, between 10° and 15°N, similar to what we see over a slightly larger domain (Fig. A2). However, the correlation (not shown) between our heat content and the assimilated product heat content in the upper 125 m is not statistically significant in this part of the basin. With deeper levels antiphase with the near surface, heat content may be very sensitive to the maximum depth of integration and this could be influencing the comparisons.

REFERENCES

Capotondi, A., and M. A. Alexander, 2001: Rossby waves in the tropical North Pacific and their role in decadal thermocline variability. *J. Phys. Oceanogr.,* **31,** 3496–3515.

Carton, J. A., X. Cao, B. S. Giese, and A. M. da Silva, 1996: Decadal and interannual SST variability in the tropical Atlantic. *J. Phys. Oceanogr.,* **26,** 1165–1175.

——, M. Chepurin, X. Cao, and B. Giese, 2000: A simple ocean data assimilation analysis of the global upper ocean, 1950–95. Part I: Methodology. *J. Phys. Oceanogr.,* **30,** 294–309.

Chang, P., L. Ji, and H. Li, 1997: A decadal climate variation in the tropical Atlantic Ocean from thermodynamics and air–sea interactions. *Nature,* **385,** 516–518.

——, R. Saravanan, L. Ji, and G. C. Hegerl, 2000: The effect of local sea surface temperatures on the atmospheric circulation over the tropical Atlantic sector. *J. Climate,* **13,** 2195–2216.

——, L. Ji, and R. Saravanan, 2001: A hybrid coupled model study of tropical Atlantic variability. *J. Climate,* **14,** 361–390.

Clarke, A. J., and A. Lebedev, 1997: Interannual and decadal changes in equatorial wind stress in the Atlantic, Indian, and Pacific Oceans and the Eastern Ocean Coastal Response. *J. Climate,* **10,** 1722–1729.

Conkright, M. E., and Coauthors, 1998: *Temperature.* Vol. 5, *World Ocean Database 1998,* CD-ROM Scientific Dataset, Version 1.0, National Oceanographic Data Center Internal Rep. 14.

Czaja, A., P. van der Vaart, and J. Marshall, 2002: A diagnostic study of the role of remote forcing in tropical Atlantic variability. *J. Climate,* **15,** 3280–3290.

Dommenget, D., and M. Latif, 2000: Interannual to decadal variability in the tropical Atlantic. *J. Climate,* **13,** 777–792.

Doney, S. C., S. Yeager, G. Danabasoglu, W. G. Large, and J. C. McWilliams, 2003: Modeling global oceanic interannual variability (1958–1997): Simulation design and model-data evaluation. NCAR Tech. Rep. NCAR/TN-452+STR, 48 pp.

Enfield, D. B., and D. A. Mayer, 1997: Tropical Atlantic SST variability and its relation to El Niño–Southern Oscillation. *J. Geophys. Res.,* **102,** 929–945.

Frankignoul, C., 1999: A cautionary note on the use of statistical atmospheric models in the middle latitudes: Comments on "Decadal variability in the North Pacific as simulated by a hybrid coupled model." *J. Climate,* **12,** 1871–1872.

——, and K. Hasselmann, 1977: Stochastic climate models. Part II: Application to sea-surface temperature anomalies and thermocline variability. *Tellus,* **29,** 284–305.

——, and E. Kestenare, 2002: The surface heat flux feedback. Part 1: Estimates from observations in the Atlantic and the North Pacific. *Climate Dyn.,* **19,** 633–647.

——, ——, M. Botzet, A. F. Carril, H. Drange, A. Pardens, L. Terray, and R. Sutton, 2004: An intercomparison between the surface heat flux feedback in five coupled models, COADS, and the NCEP reanalysis. *Climate Dyn.,* **22,** 373–388.

Gent, P. R., and J. C. McWilliams, 1990: Isopycnal mixing in ocean circulation models. *J. Phys. Oceanogr.,* **20,** 150–155.

——, J. Willebrand, T. J. McDougall, and J. C. McWilliams, 1995: Parameterizing eddy-induced tracer transports in ocean circulation models. *J. Phys. Oceanogr.,* **25,** 463–474.

——, F. O. Bryan, G. Danabasoglu, S. C. Doney, W. R. Holland, W. G. Large, and J. C. McWilliams, 1998: The NCAR Climate System Model global ocean component. *J. Climate,* **11,** 1287–1306.

Hanawa, K., P. Rual, R. Bailey, A. Sy, and M. Szabados, 1995: A new depth-time equation for Sippiocan TSK T-7, T-6, and T-4 expendable bathythermographs (XBT). *Deep-Sea Res.,* **A8,** 1423–1451.

Hastenrath, S., 1990: Decadal-scale changes of the circulation in the tropical Atlantic sector associated with Sahel drought. *Int. J. Climatol.,* **10,** 459–472.

Hellerman, S., and M. Rosenstein, 1983: Normal monthly wind stress over the World Ocean with error estimates. *J. Phys. Oceanogr.,* **13,** 1093–1104.

Houghton, R. W., 1991: The relationship of sea surface temperature to thermocline depth at annual and interannual time scales in the tropical Atlantic Ocean. *J. Geophys. Res.,* **96,** 15 173–15 185.

——, and Y. Tourre, 1992: Characteristics of low-frequency sea sur-

face temperature fluctuations in the tropical Atlantic. *J. Climate,* **5,** 765–771.

Joyce, T. M., 1988: On the wind-driven cross-equatorial flow in the Atlantic Ocean. *J. Phys. Oceanogr.,* **18,** 793–799.

——, C. Deser, and M. A. Spall, 2000: The relation between decadal variability of subtropical mode water and the North Atlantic Oscillation. *J. Climate,* **13,** 2550–2569.

Kalnay, E., and Coauthors, 1996: The NCEP/NCAR 40-Year Reanalysis Project. *Bull. Amer. Meteor. Soc.,* **77,** 437–471.

Katz, E. J., 1993: An interannual study of the Atlantic North Equatorial Countercurrent. *J. Phys. Oceanogr.,* **23,** 116–123.

Kushnir, Y., R. Seager, and J. Miller, 2002: A simple coupled model of tropical Atlantic decadal climate variability. *Geophys. Res. Lett.,* **29,** 2133, doi:10.1029/2002GL015874.

Large, W. G., and P. R. Gent, 1999: Validation of vertical mixing in an equatorial ocean model using large eddy simulations and observations. *J. Phys. Oceanogr.,* **29,** 449–464.

——, G. Danabasoglu, and S. Doney, 1997: Sensitivity to surface forcing and boundary layer mixing in a global ocean model: Annual-mean climatology. *J. Phys. Oceanogr.,* **27,** 2418–2447.

——, ——, J. C. McWilliams, P. R. Gent, and F. O. Bryan, 2001: Equatorial circulation of a global ocean climate model with anisotropic horizontal viscosity. *J. Phys. Oceanogr.,* **31,** 518–536.

Mehta, V. M., 1998: Variability of the tropical ocean surface temperatures at decadal-multidecadal timescales. Part I: The Atlantic Ocean. *J. Climate,* **11,** 2351–2375.

Mélice, J.-L., and J. Servain, 2003: The tropical Atlantic meridional SST gradient index and its relationships with the SOI, NAO, and Southern Ocean. *Climate Dyn.,* **20,** 447–464.

Merle, J., and S. Arnault, 1985: Seasonal variability of the surface dynamic topography in the tropical Atlantic Ocean. *J. Mar. Res.,* **43,** 267–288.

Moura, D. W., and J. Shukla, 1981: On the dynamics of droughts in northeast Brazil: Observations, theory and numerical experiments with a general circulation model. *J. Atmos. Sci.,* **38,** 2653–2675.

Nobre, P., and J. Shukla, 1996: Variations of sea surface temperature,

wind stress, and rainfall over the tropical Atlantic and South America. *J. Climate,* **9,** 2464–2479.

Philander, S. G., 1989: *El Niño, La Niña, and the Southern Oscillation.* Academic Press, 293 pp.

Qiu, B., and T. M. Joyce, 1992: Interannual variability in the mid- and low-latitude western North Pacific. *J. Phys. Oceanogr.,* **22,** 1062–1079.

Reynolds, R. W., and T. M. Smith, 1994: Improved global sea surface temperature analysis using optimum interpolation. *J. Climate,* **7,** 929–948.

Ruiz-Barradas, A., J. A. Carton, and S. Nigam, 2000: Structure of interannual-to-decadal climate variability in the tropical Atlantic sector. *J. Climate,* **13,** 3285–3297.

Seager, R., Y. Kushnir, P. Chang, N. Naik, J. Miller, and W. Hazeleger, 2001: Looking for the role of the ocean in tropical Atlantic decadal climate variability. *J. Climate,* **14,** 638–655.

Servain, J., 1991: Simple climatic indices for the tropical Atlantic Ocean and some applications. *J. Geophys. Res.,* **96,** 15 137–15 146.

——, G. Clauzet, and I. C. Wainer, 2003: Modes of tropical Atlantic climate variability observed by PIRATA. *Geophys. Res. Lett.,* **30,** 8003, doi:10, 1029/22002GL015124.

Smith, S. R., D. M. Legler, and K. V. Verzone, 2001: Quantifying uncertaintities in NCEP reanalysis using high-quality research vessel observations. *J. Climate,* **14,** 4062–4072.

Sutton, R. T., S. P. Jewson, and D. P. Rowell, 2000: The elements of climate variability in the tropical Atlantic region. *J. Climate,* **13,** 3261–3284.

White, W. B., 1995: Design of a global observing system for the gyre-scale upper ocean temperature variability. *Progress in Oceanography,* Vol. 36, Pergamon, 169–217.

Xie, S.-P., 1999: A dynamic ocean–atmosphere model of the tropical Atlantic decadal variability. *J. Climate,* **12,** 64–70.

Yang, J., 1999: A linkage for decadal climate variations in Labrador Sea and the tropical Atlantic Ocean. *Geophys. Res. Lett.,* **26,** 1023–1026.

Zhou, Z., and J. Carton, 1998: Latent heat flux and interannual variability of the coupled atmosphere–ocean system. *J. Atmos. Sci.,* **55,** 494–501.